PCCP

Accepted Manuscript

ROYAL SOCIETY OF CHEMISTRY

www.rsc.org/pccp

Journal Name

RSCPublishing

ARTICLE

The electronic, optical and magnetic consequences of delocalization in multifunctional donor-acceptor organic polymers

Cite this: DOI: 10.1039/xoxxoooooox

Received ooth January 2012,
Accepted ooth January 2012

DOI: 10.1039/xoxxoooooox

www.rsc.org/

Felix J. Rizzuto,[a] Carol Hua,[a] Bun Chan,[a] Thomas B. Faust,[a] Aditya Rawal,[b] Chanel F. Leong,[a] James M. Hook,[b] Cameron J. Kepert [a] and Deanna M. D'Alessandro[a*]

Two organic polymers containing alternating electron donating triarylamine and electron accepting thiazolo[5,4-*d*]thiazole (TzTz) moieties have been synthesized and their redox states investigated. When donor and acceptor units are proximal (polymer **1**), electron density is delocalized, leading to a small electrical and optical band gap; these are larger with the inclusion of an adjoining alkynyl-phenyl bridge (polymer **2**), where electron density is more localized due to the rotation of the monomer units. As a result, **1** and **2** display different optical and fluorescence properties in their neutral states. Upon chemical and electrochemical redox reactions, radicals form in both **1** and **2**, yielding magnetic materials that display temperature-independent paramagnetism, attributable to delocalization of radical spins along the polymeric backbones. The ability to convert between diamagnetic and paramagnetic states upon chemical oxidation and/or reduction allows for the materials to display switchable magnetism and fluorescence, imparting multifunctionality to these solid-state purely organic materials.

Introduction

Owing to the successful integration of redox-active moieties and free radical species, organic polymers have recently shown great promise as potential components in conductive devices.[1,2] As a popular means of facilitating electrical mobility, the assimilation of aromatic functionalities capable of redox chemistry into polymeric backbones has led to the creation of materials displaying semiconductivity, with prospective applications in field effect transistors and electroactive technologies.[3,4] In recent years, particular attention has focused on one-dimensional polymers composed of alternating electron donating and accepting moieties. These have been implicated in photovoltaic devices due to favorable optical and electronic properties resulting from charge movement along conjugated redox-active units.[5-9]

While covalent organic polymers are typically amorphous, they often exhibit nanoporosity and respectable surface areas, which have led to their proposed applications in gas storage and absorptive separation.[10-12] Metal-doping, post-synthetic modifications and pore size tailoring have likewise been achieved,[13] leading to materials with intriguing electronic properties and host-guest chemistry.[12,14,15] With respect to radical systems in particular, permanently high spin ferromagnetic polymers have been synthesized[16,17] and some display dual magnetic and conductive behavior.[18]

As a subset of this organic class of polymers, two-dimensional, insoluble polymer systems are of particular interest, as they provide a platform for the synthesis of solid-state organic electrical devices. Holistically, they are often highly robust, hydrophobic and relatively straightforward to synthesize, making them important candidates for integration into utilitarian devices.[19]

Towards the aim of achieving multifunctional electronic, optical and magnetic materials, the synthesis of electroactive systems that can reversibly switch between different electronic states is key. The ability to access a range of oxidation states allows a given material to exhibit diverse magnetic, conductive and optical properties that would otherwise be inaccessible in its as-synthesized state.[12,20] This has been investigated extensively for inorganic materials, but to a more limited extent in organic systems.

Herein, we detail the synthesis of two polymers incorporating the electron accepting thiazolo[5,4-*d*]thiazole (TzTz) and electron donating triarylamine moieties. In **1**, the donor and acceptor units are proximal, while they are separated by alkynyl connectors in **2** (Scheme 1). The increased distance

between donor and acceptor functionalities in **2** was investigated as a means of tuning the electronic and optical properties of these moieties, as well as their response to external electrical and magnetic stimuli.

Results and Discussion

Synthesis and characterization

1 was synthesized by a condensation reaction between tris(4-formyl)phenylamine and dithiooxamide in DMF, while **2** was synthesized from a Sonogashira-Hagihara palladium cross coupling reaction between tris(4-ethynylphenyl)amine and 2,5-bis(4-bromophenyl)thiazolo[5,4-*d*]thiazole (Scheme 1).

Both polymers were characterized by solid state NMR, and similar features were observed in the ^{13}C CP-TOSS spectra (Fig. 1). The signals are better resolved in the case of **2** as compared to **1**, which may indicate a higher degree of molecular mobility associated with the linker chains in **2**. The broad peak at *ca.* 148 ppm in **1** may be assigned to the N–C carbon in the triphenylamine moiety and the carbon from the TzTz moiety that is bonded to the aromatic ring. In the case of **2**, which has a higher mobility, the 148 ppm peak is indeed resolved into two corresponding peaks at 150 and 146 ppm. Additionally, the single broad aromatic peak at 129 ppm in **1** is also resolved into two peaks at 133 and 126 ppm, which are assigned to the non-protonated and protonated aromatic species, respectively (Fig. S3). The broad shoulder at *ca.* 115 ppm for both **1** and **2** corresponds to the protonated aromatic carbon species that are *ipso* to the N–C carbon in the triphenylamine moiety. For **1**, a weak signal at 190 ppm indicates the presence of unreacted aldehyde, which is corroborated by the FTIR signal at 1695 cm^{-1} (Fig. S2). In the case of **2** the peaks between 75 to 90 ppm represent distinct quaternary alkynyl carbons, which was taken as an indicator of successful cross coupling of the monomer units in **2**. This assignment was verified by the presence of similar resonances in the ^{13}C non-quaternary (NQS) MAS spectrum, where the resonances of all protonated sp^2 carbons (as there are no sp^3 carbons present in either polymer) have been suppressed (Fig. S3). The signal at 3296 cm^{-1} in the FTIR spectrum of **2** indicates the presence of residual unreacted alkynyl species.

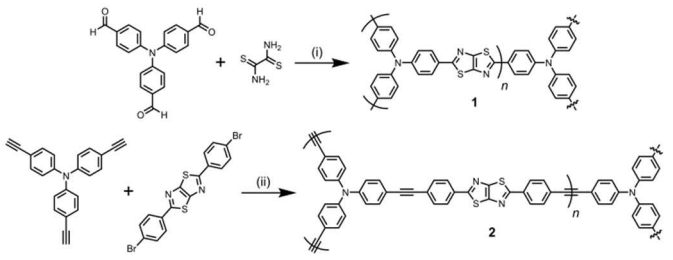

Scheme 1 Synthesis of **1** and **2**, showing the electron donating bis(triarylamine) unit connected by electron accepting TzTz bridges. Reagents and conditions: (i) DMF, reflux, 4 h. (ii) $Pd(PPh_3)_4$, CuI, Et_3N/DMF, 90 °C, 3 days. The monomers have been expanded to give a representation of fragments **1m** and **2m**, used in proceeding DFT calculations.

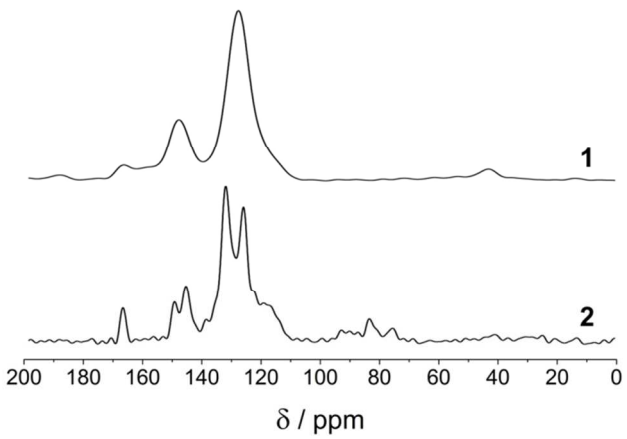

Fig. 1 Solid State ^{13}C CPMAS NMR spectra of **1** and **2**.

Both **1** and **2** were amorphous and insoluble in common organic solvents, as expected for this class of cross-linked, interwoven 2D organic polymer, in which monomer control is absent. The thermal gravimetric analysis conducted on **1** and **2** (Fig. S1) revealed thermal stability up to 250 °C. Pore volume was analyzed by nitrogen adsorption isotherms obtained at 77 K (Fig. S4). The BET surface area for **1** was determined to be 178(1) m^2 g^{-1} while **2** was found to be non-porous. In the adsorption isotherm of **1**, a maximum N_2 uptake of 9.1 mmol g^{-1} was reached at 0.95 bar. The pore size analysis revealed a predominant pore size of 15 Å, while pores with a 26 Å diameter were also present (Fig. S5). The nitrogen isotherm for **1** furthermore showed significant hysteresis, which may be indicative of flexibility in the polymer networks.

Electrochemistry

Solid state cyclic voltammetry (CV) was performed on **1** and **2** in $[(n\text{-}C_4H_9)_4N]PF_6$/MeCN electrolyte (Fig. 2). For **1**, one broad quasi-reversible redox process was observed at 0.98 V *vs.* Fc/Fc$^+$, corresponding to oxidation of the triarylamine core to its radical cation. The splitting of this redox wave into two processes at a scan rate of 100 mV s^{-1} may be indicative of a short-lived mixed-valence bis(triarylamine) state, although the same process was not observed at other scan rates (Fig. S6). Akin to the conclusions of previous reports,[12] we attribute the broad oxidation processes to the sequential generation of radical cation and dication species. The quasi-reversible redox process at 1.30 V *vs.* Fc/Fc$^+$ in the anodic region of **2** is likewise ascribed to the formation of an aminium radical cation and the respective dication species.

In the cathodic sweep of **1**, one reversible and one quasi-reversible reduction process were observed at –1.33 and –1.78 V *vs.* Fc/Fc$^+$, respectively. These processes are ascribed to the sequential one and two electron reductions of the TzTz core. With respect to the first cathodic process, the large peak separation between the forward and reverse waves (ΔE = 0.88 V) may be indicative of structural flexibility upon reduction, resulting in a change in the polymer structure.[21] This flexibility in the polymer chains is consistent with the observation of

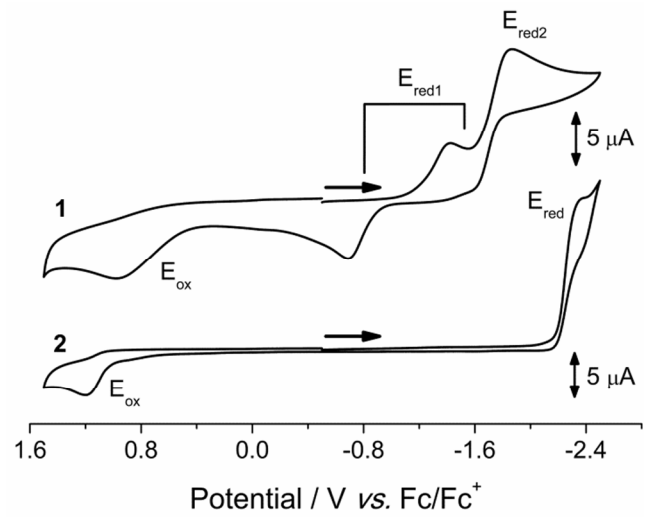

Fig. 2 Solid state CVs of **1** and **2** in $[(n\text{-}C_4H_9)_4N]PF_6$/MeCN at a scan rate of 50 mV s^{-1}. The arrows indicate the direction of the forward scan.

hysteresis in the 77 K N_2 gas sorption isotherm (Fig. S4) and may arise from the reversible, but slow, intercalation of countercations during the forward and reverse scans (where $i_{p,rev}/i_{p,fwd} = 0.98$).

In the cathodic region of **2**, only one reduction process is observed at –2.26 *vs.* Fc/Fc^+, as compared to the two processes observed in **1**. This difference in reduction properties may be attributed to the differential conjugation in the two systems. The relatively more aromatic polymer **1** provides a higher level of stabilization for the reduced TzTz core (*i.e.*, the excess electron density is delocalized through the entire polymer system) while **2** is less aromatic due to the presence of the alkynyl bridges. This reduces the ability of **2** to delocalize the excess electron density resulting from the reduction of the TzTz moiety, such that the first reduction process is considerably more difficult than in **1**.

The electrical band gap was calculated from the potential difference between the onset of the first oxidation (HOMO) and the first reduction (LUMO) process, using established equations.[22,23] For **1**, the HOMO–LUMO band gap is 1.61 eV; for **2**, it is 2.88 eV.

Estimations of the optical band gaps were achieved by Tauc plots, constructed from the solid state vis-NIR spectra of **1** and **2** (Fig. S7 and S8). The optical band gap of **1** was 1.76 eV, and that of **2** was 2.25 eV. These correspond with the electrical band gaps calculated from the voltammograms in Fig. 2, indicating that the energy between the HOMO and LUMO is significantly smaller in **1** than it is in **2**.

The reason for this difference was investigated by DFT calculations and, in particular, the distribution of electron density in the molecular orbitals of **1** and **2**. The DFT calculations show that the additional linkers in the monomer of **2** (denoted **2m**) have led to a significant structural effect when compared to the corresponding monomer of **1** (denoted **1m**) (Fig. 3). Thus, rotation of the triarylamine moieties with respect to the TzTz core has become more facile upon the introduction of the alkynyl linkers, with the rotated structure of **1m** (denoted **1mR**) being higher in energy than the equilibrium structure by 42 kJ mol^{-1}, whereas for **2m** the corresponding energy change (to the rotated structure, denoted **2mR**) is just 6 kJ mol^{-1}. These results from the DFT are in agreement with the observed motional line narrowing seen in the ^{13}C NMR spectrum for **2**, as compared to the broad signals seen for **1**. In terms of molecular orbitals, we find that, as expected, the turning of the triarylamine units leads to a disruption of the delocalization, such that the HOMOs of both **1mR** and **2mR** are centered on the amine units. We also note that, although the three aryl groups surrounding the central nitrogen are not coplanar, the amine-centered molecular orbitals are still largely delocalized over all three aryl moieties.

The DFT electron affinities for **1m**, **1mR**, **2m** and **2mR** are 97, –22, 146 and 134 kJ mol^{-1}, respectively. Thus, in the equilibrium structures **1m** and **2m**, the reduction is more favorable with the alkynyl-linked monomer **2m** (electron affinity (EA) = 146 kJ mol^{-1} *vs.* 97 kJ mol^{-1} for **1m**), which is in contrast to the experimental observation that the reduction of polymer **1** is more favorable. In polymer **1**, however, we can expect that the more extensive delocalization will substantially increase the EA when compared with that for **1m**. We note that the EA of 134 kJ mol^{-1} for **2mR** is smaller than that for **2m**. Due to the structural flexibility of **2m**, the formation of **2** is likely to occur in the presence of a relatively abundant amount of "twisted" monomers **2mR**. The EAs of the twisted units in **2** are unlikely to be significantly different from that of **2mR** due to the localization of the orbitals. Such a proposition would account for the experimental observation of the more facile reduction of **1** and is consistent with the more densely packed structure of **2**, implied by the porosity data.

The experimental band gap for **1** is smaller than that for **2**. The DFT value for **1m** (289 kJ mol^{-1}) is, however, larger than that for **2m** (258 kJ mol^{-1}), but it is comparable to that for **2mR** (274 kJ mol^{-1}). Thus, the comparison between experimental

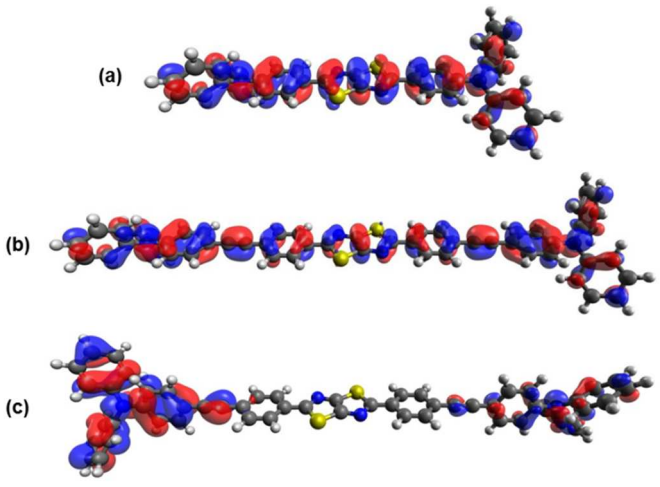

Fig. 3 HOMOs for the monomer fragments of **1** and **2**: (a) **1m**, (b) **2m**, and (c) **2mR**. While delocalized in their "planar" forms, "twisting" of the monomer fragments leads to charge localization on the triarylamine units.

band gaps for the polymers and the theoretical values for the monomers also points toward the polymer **1** being dominated by "planar" monomers **1m**, while **2** is composed of a significant amount of "twisted" monomers **2mR**. The delocalization of **1m** units within **1** should lead to a lower band gap than that for a single monomer. On the other hand, we would not expect the rotated **2mR** units in **2** to have notably different band gaps than that for the isolated monomeric **2mR**. As a result, the process of polymerization can be expected to, at some stage, bring the band gap of **1** to a level lower than that of **2**.

Solid state spectroelectrochemistry

Solid state spectroelectrochemistry (SEC)[24] experiments were conducted on **1** and **2** in $[(n\text{-}C_4H_9)_4N]PF_6$/MeCN electrolyte during oxidation (Fig. 4) and reduction (Fig. S9 and S10) to investigate the relationship between the optical and electronic properties of the polymers. For the neutral species, the bands above 19000 cm^{-1} can be assigned to π(HOMO) → π*(LUMO) transitions. The application of an anodic potential to **2** resulted in a decrease of the π → π* bands, indicating a depopulation of the HOMO, and the appearance of a broad band centered at *ca.* 12500 cm^{-1}, assigned to the D_0 to D_1 transition of the triarylamine radical cation. During the oxidation of **1**, both π → π* transitions likewise decrease (as with **2**), and the shoulder band at *ca.* 16000 cm^{-1} increases in intensity.

Upon oxidation, the characteristic triarylamine radical band observed for **2** in the region 8000-15000 cm^{-1} is not observed in **1**. This observation may be rationalized on the basis of the higher degree of delocalization in **1**, which leads to oxidation from a highly delocalized HOMO.

A comparison between the spectral progressions accompanying these transitions is provided in Fig. 4. In general, the appearance of two stable isosbestic points in both experiments indicates that the polymers are stable to electrogeneration, and that both the TzTz and triarylamine moieties are involved in the oxidation process. Notably, the gap between the two points is greater in the oxidation of **2** than in **1**, again reflective of the decreased proximity between electron donating and accepting units.

Investigations into the electronic excitation properties with TD-DFT indicated that the major UV-vis absorption bands for neutral **1m** and **2m** in the 20000-25000 cm^{-1} range are dominated by transitions from delocalized HOMOs to TzTz-centered LUMOs. For neutral **2mR**, however, the major band in this range corresponds to the HOMO *within* the TzTz unit to its LUMO. Once oxidized, new bands in the 10000-15000 cm^{-1} range emerge for both **2m** and **2mR**. In the case of **2m**, this is due to a transition from an orbital that is mainly centered at the triarylamine units to a delocalized orbital. For **2mR**, the disruption of the conjugation results in a transition in the same range, but it originates from a triarylamine-centered orbital to an acceptor orbital at the TzTz core. In contrast to **2m** and **2mR**, oxidation of **1m** does not lead to a transition in the 10000-15000 cm^{-1} window. Its major absorption instead occurs at 21364 cm^{-1}, which is assigned to a transition from the delocalized HOMO to a TzTz-centered orbital. Therefore, as a result of the differing degrees of delocalization, the oxidation of **1** results in a higher energy optical band than in **2**, commensurate with the SEC data.

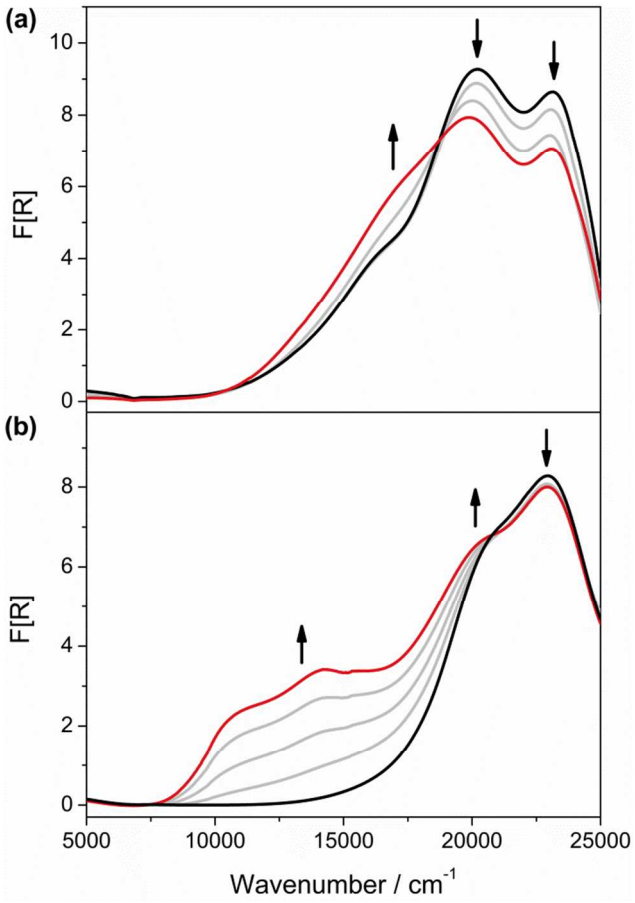

Fig. 4 *In situ* oxidative solid state vis-NIR SEC conducted on polymers **1** (a) and **2** (b) in $[(n\text{-}C_4H_9)_4N]PF_6$/MeCN electrolyte over the range 5000-25000 cm^{-1}. Arrows show the direction of spectral progression.

No new spectral transitions were observed during the reduction of **1** or **2**. The disappearance of the shoulder band of **1** at *ca.* 16500 cm^{-1} was the only shift observed in the reduction of **1** (Fig. S9).

Chemical redox reactions

Clarification of the solid state SEC data was accomplished by obtaining UV-vis-NIR spectra on samples oxidized *ex situ*. Chemical oxidation of the polymers with an excess of $NOPF_6$/MeCN (0.87 V *vs.* Fc/Fc^+)[25] resulted in a color change from red (**1**) and dark yellow (**2**) to black in both cases. Spectroscopically, this change manifested as a broad band at *ca.* 15000 and 12500 cm^{-1} for **1** and **2**, respectively (Fig. 5), in good agreement with the SEC data (Fig. 4). The presence of a broad band in the NIR region of **1** after chemical oxidation is reminiscent of an intervalence charge transfer (IVCT) band; however, subsequent investigation by mid-FTIR spectroscopy revealed no such transition. Comparison of the UV-vis transition intensities between the electrochemically and *ex situ*

oxidized samples indicated complete conversion to the oxidized species for both **1** and **2**.

Addition of an excess of reductant (LiNp/THF, –3.10 V *vs.* Fc/Fc^{+})[25] resulted in no significant color change in either **1** or **2**, in agreement with the SEC. The spectral change in both species during reduction is minimal: the shoulder band of **2** at 21500 cm^{-1} increased and that of **1** at 15600 cm^{-1} decreased with respect to the neutral species. Normalized UV-vis-NIR spectra for neutral, oxidized and reduced samples of **1** and **2** are presented in Fig. 5.

Magnetism

Variable temperature magnetic data were collected on the oxidized and reduced samples of **1** and **2** over the range 2-300 K at 1 kOe (Fig. 6). Molar masses were taken from the 'repeatable' units of the polymeric system (Fig. S11 and S12); however, given the incomplete reaction of aldehyde and alkynyl groups in **1** and **2**, respectively, the values reported hereafter are not absolute.

In their oxidized forms, both **1** and **2** exhibit a monotonic linear decrease in $\chi_M T$ with decreasing temperature, suggesting that spins align in an antiparallel fashion. Notably, the Curie Weiss Law is not obeyed up to 300 K, nor can a dimer

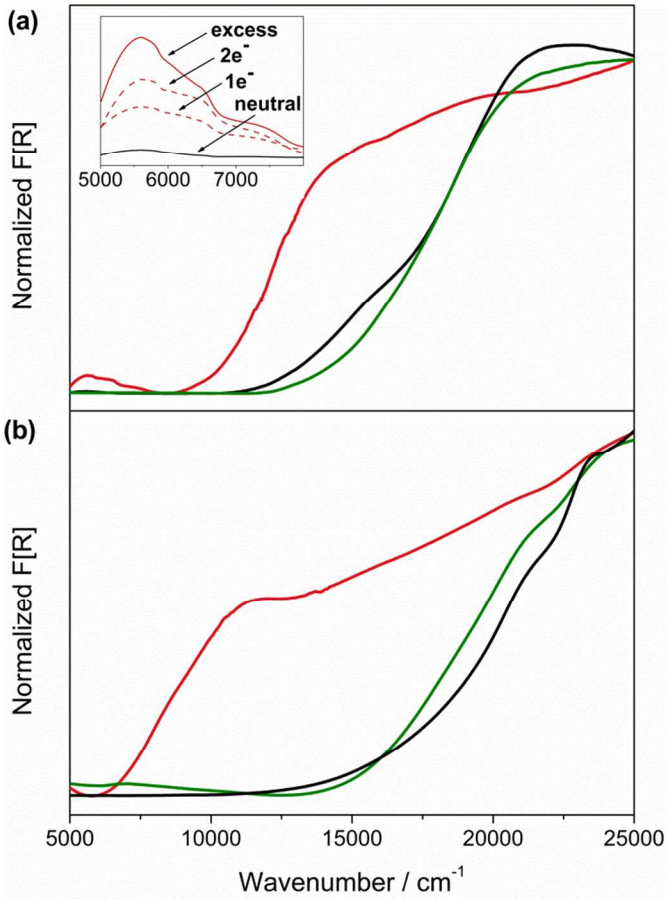

Fig. 5 Solid state vis-NIR spectra collected on neutral (black), oxidized (red) and reduced (green) samples of **1** (a) and **2** (b). The inset in (a) is the transition observed between 5000-8000 cm^{-1} in **1** oxidized with $1e^{-}$, $2e^{-}$ and excess equivalents of $NOPF_6$ in MeCN.

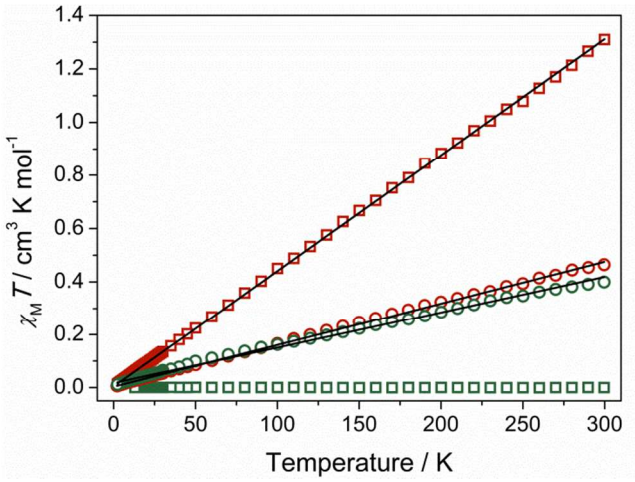

Fig. 6. Variable temperature magnetic susceptibility data over the range 2-300 K under an applied field of 1 kOe for oxidized (red) and reduced (green) samples of **1** (circles) and **2** (squares). The lines are the best fit to the data according to the equation $\chi_M T = \chi_{TIP} T$.

(Bleaney-Bowers) or alternating S = 1/2 magnetic chain (Bonner-Fisher) model be fit to the data. Instead, a temperature-independent paramagnetism (TIP) term (*i.e.*, $\chi_M T = \chi_{TIP} T$) was used to quantify the relative magnetic properties of each polymer. Upon oxidation, **1** displays a temperature-independent moment of 1.57×10^{-3} cm^3 mol^{-1}; it exhibits a TIP value of 1.34×10^{-3} cm^3 mol^{-1} in its reduced form. Conversely, the oxidation of **2** results in a larger TIP term of 4.36×10^{-3} cm^3 mol^{-1} whilst reduced **2** is diamagnetic. This may be due to the limited diffusion of the naphthalenide radical anion through the non-porous polymer structure, whereas the porosity and structural flexibility of **1** allows for penetration of the reducing agent through the pores of the material.

The presence of TIP indicates one of two possibilities with respect to the distribution of radical spins: a) the magnetic ground state is coupled with non-thermally populated excited states (van Vleck TIP); or b) the unpaired electrons are delocalized, creating a Fermi gas-like state (Pauli paramagnetism). In the former case, near-degeneracy of the radical singly-occupied orbitals would promote fluctuation between energy levels, facilitating van Vleck TIP. This phenomenon, however, is almost exclusively attributed to metal *d*-orbital spins and is typically small in magnitude. While heterogeneous oxidation/reduction would create domains of radical concentration and potentially facilitate magnetic coupling between neutral and radical states, the magnetism of electronically-transformed **1** and **2** is more appropriately ascribed to delocalized radical spins. This would distribute charge evenly along the polymer backbone, preventing exchange coupling, and would lead to Pauli paramagnetism. Delocalized singly-occupied HOMOs are furthermore consistent with the DFT calculations for both **1** and **2**.

Classically, the density of states for localized spins is represented by a Fermi-Dirac distribution. As such, maximum χ_{TIP} values are theoretically restricted to the room temperature

χ_M exhibited by a single, localized S = 1/2 spin. While redox-transformed **1** exhibits χ_{TIP} and room temperature χ_M values consistent with this, significant deviation of χ_{TIP} from the saturated S = 1/2 value is seen in oxidized **2**. With a mixture of delocalized and localized HOMOs in **2** (resulting from a combination of the **2m** and **2mR** monomer units), radical spins on the polymer will be delocalized in some regions and concentrated in domains in others. The net $\chi_M T$ is therefore a result of this mixed-HOMO character.

Fluorescence

A second notable consequence of chemical redox reactions was a change in the fluorescent character of **2**. While **1** was not fluorescent, **2** displayed different emission spectra when excited at the absorption energies of its respective redox-active moieties (Fig. 7). When excited from the UV band at 28090 cm^{-1}, three peaks were observed at 25000 and 23920 and 22470 cm^{-1}. This progression corresponds to the N–C stretching normal modes of aromatic amines (frequency range of 1335 to 1250 cm^{-1}), indicating that this emission comes from the HOMO localized on the triarylamine moiety (*i.e.*, monomer fragments corresponding to **2mR**). This was further confirmed by inspection of the absorption spectrum of the triarylamine monomer component of **2**, which displayed no absorption bands in the visible region.

When excited at 22760 cm^{-1}, the emission spectrum of neutral **2** displayed two redshifted fluorescence maxima at 21550 and 19760 cm^{-1}, corresponding to the fluorescence of the delocalized HOMO (*i.e.*, the charge delocalized monomer fragments **2m**). As such, the isolation of the donor and acceptor functionalities in **2** also isolates the fluorescence of the respective moieties. In solution, the monomer components of **2** each fluoresce blue (maxima centered *ca.* 25000 cm^{-1}), while **2** itself fluoresces both blue and green, depending on the excitation wavelength. The decrease in energy associated with polymerization is attributable to a decrease in the HOMO–LUMO band gap, reflective of the increased conjugation of **2**.

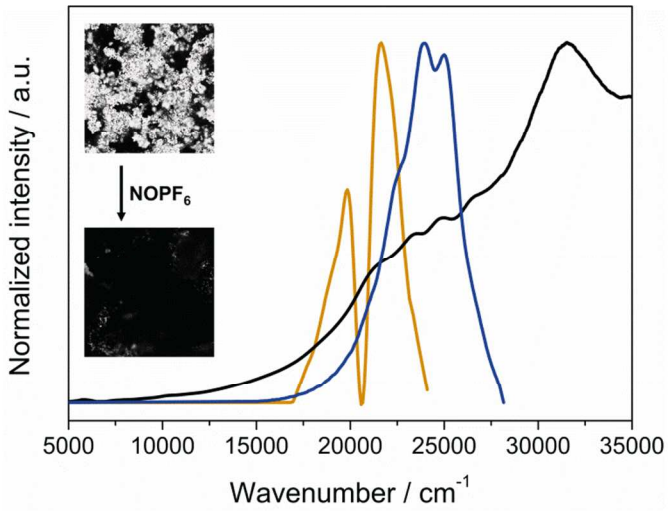

Fig. 7 An overlay of the absorbance spectrum of **2** (black), the emission spectrum of **2** excited at 28090 cm^{-1} (blue), and the emission spectrum of **2** excited at 22760 cm^{-1} (yellow). Pictorial inset is confocal microscopy images of **2** excited at 410 nm, showing the quenching of the fluorescence upon reaction with excess $NOPF_6$, due to the formation of the radical species.

The fluorescence of **2** was quenched upon oxidation and the formation of a radical species. Notably, this was not homogeneous, and domains of fluorescent material identified by confocal microscopy indicated incomplete conversion to the oxidized phase, as expected for the non-porous polymeric system.

Conclusions

Two polymeric systems differing in the distance between their electron donating and accepting units undergo switching between their diamagnetic and paramagnetic states upon chemical redox reactions. During oxidation, prominent color changes are observed due to the formation of a radical aminium cation, while reduction caused no significant optical change.

Variable temperature magnetic measurements indicated a dominant temperature-independent paramagnetism for all successfully redox-transformed materials, resulting from the delocalization of radical spins. This was further confirmed by DFT calculations, which indicated that, structurally speaking, **2** was composed of a high percentage of "twisted" monomers, while **1** was composed of "planar" units. This resulted in a higher degree of delocalization in **1**, leading to a lower reduction potential, lower optical/electrical band gap and a higher energy optical transition upon oxidation.

In switching from diamagnetic to paramagnetic states, the optical, magnetic and fluorescence properties of these materials were markedly altered. This was exemplified most prominently by **2**, which is fluorescent in its neutral state, and not fluorescent upon oxidation. Hence, utility is a function of redox state. With the ability to convert between fluorescent and magnetic states upon oxidation, **1** and **2** can be chemically or electrochemically switched to their radical species, accessing magnetic properties that would otherwise be absent in their neutral states.

Experimental Section

Tris(4-ethynylphenyl)amine,[26] $Pd(PPh_3)_4$,[27] tris(4-formylphenyl)amine[28] and 2,5-bis(4-bromophenyl)thiazolo[5,4-*d*]thiazole[29] were synthesized according to literature procedures. Distilled and degassed MeCN (dried over CaH_2) was used for all experiments requiring MeCN. DMF and Et_3N were dried over CaH_2 before use. All other reagents and solvents used were obtained commercially and used without further purification. Microanalyses were carried out at the Chemical Analysis Facility – Elemental Analysis Service in the Department of Chemistry and Biomolecular Science at Macquarie University, Australia.

Poly(triarylamine-thiazolo[5,4-*d*]thiazole) (1). Dithiooxamide (110 mg, 0.90 mmol), and tris(4-formylphenyl)amine (100 mg, 0.30 mmol) were refluxed in DMF (10 mL) for 4 h. The mixture was filtered and the solid

washed with H_2O and MeOH. The polymer was further washed with MeOH in a Soxhlet extraction over 48 h before being dried under vacuum. A red solid was obtained (170 mg). UV-vis-NIR (solid state): 42280, 22770, 15990 cm^{-1}. IR (KBr): 1668, 1593, 1506, 1323, 1176, 831 cm^{-1}. Elemental analysis: C 61.84, H 3.48, N 11.12, S 17.08%.

Poly(triarylamine-alkynylphenyl-thiazolo[5,4-*d*]thiazole) (2). Tris(4-ethynylphenyl)amine (200 mg, 0.630 mmol), 2,5-bis(4-bromophenyl)thiazolo[5,4-*d*]thiazole (228 mg, 0.504 mmol) and $Pd(PPh_3)_4$ (5.8 mg, 5.04 μmol, 1 mol%) were added to a mixture of Et_3N (5 mL) and DMF (5 mL). The resulting yellow suspension was stirred for 5 min at room temperature under N_2. Copper iodide (1.92 mg, 0.0101 mmol, 2 mol%) was then added and the reaction mixture heated at 90 °C for 3 days. The resulting dark reaction mixture was filtered and washed successively with DMF, CH_3Cl, MeOH, H_2O, MeOH and Ac_2O. The solid was then washed in a Soxhlet extraction with MeOH overnight and dried under vacuum to yield a yellow solid (280 mg). UV-vis-NIR (solid state): 36810, 31340, 22950, 20830 cm^{-1}. IR (KBr): 3290, 2104, 2206, 1594, 1442, 1319 cm^{-1}. Elemental Analysis: C, 61.02; H, 2.81; N, 5.65; S, 12.32%.

Redox transformations

Oxidation: The neutral polymer (20.0 mg) was added to a dry and degassed saturated solution of $NOPF_6$ in MeCN (8 mL). Nitrogen gas was bubbled through the suspension for 10 min, yielding a black solid. The reaction mixture was filtered and the solid washed with MeCN before being dried under vacuum.

Reduction: The neutral polymer (30.0 mg) was suspended in a small portion of dry THF (*ca.* 3 mL) and reacted with an excess of 0.1 M lithium naphthalenide (LiNp) in THF under Ar. The product was filtered, washed with three portions of dry THF (each 10 mL) and allowed to dry.

UV-vis-NIR spectroscopy. UV-vis-NIR spectra were obtained on the samples at room temperature using a Cary 5E Spectrophotometer equipped with a Harrick Praying Mantis accessory over the wavenumber range 5000-50000 cm^{-1}. $BaSO_4$ was used for the baseline. Spectra are reported as the Kubelka-Munk transform, where $F[R] = (1-R)^2/2R$ (R is the diffuse reflectance of the sample as compared to $BaSO_4$).

FT-IR spectroscopy. Room temperature FTIR spectra were obtained using a Bruker Tensor 27 Infrared Spectrometer, over the range 500-4000 cm^{-1}. Samples were prepared in a dry, finely ground KBr matrix, on which the background was collected.

Solid state electrochemistry. Solid state electrochemical measurements were performed using a Bioanalytical Systems BAS 100A Electrochemical Analyser. Argon was bubbled through solutions of 0.1 M $[(n\text{-}C_4H_9)_4N]PF_6$ dissolved in distilled MeCN. The cyclic voltammograms (CVs) were recorded using a glassy carbon working electrode (1.5 mm diameter), a platinum wire auxiliary electrode and an Ag/Ag^+ wire quasi reference electrode. Solid state samples were mounted on the glassy carbon working electrode by dipping the electrode into a paste made of the powder sample in MeCN. The Fc/Fc^+ redox couple was used as an internal standard.

Solid state spectroelectrochemistry. In the solid state, the diffuse reflectance spectra of the electrogenerated species were collected *in situ* in a 0.1 M $[(n\text{-}C_4H_9)_4N]PF_6$/MeCN electrolyte over the range 5000-25000 cm^{-1} using a Harrick Omni Diff Probe attachment and a custom built solid state spectroelectrochemical cell described previously.[24] The cell consisted of a Pt wire counter electrode and a Ag/Ag^+ quasi reference electrode. The solid sample was immobilized onto a 0.1 mm thick Indium-Tin-Oxide (ITO) coated quartz slide (which acted as the working electrode) using a thin strip of Teflon tape (for **2**) or the addition of $LiClO_4$-intercalated PVC (to a diameter of 1 cm) (for **1**). The applied potential (from –2.0 V to 2.0 V) was controlled using an eDAQ potentiostat. Continuous scans of the sample were taken and the potential increased gradually until change in the spectrum was observed.

Solid State NMR. The ^{13}C CPMAS solid state NMR experiments were carried out on a wide-bore Bruker Biospin Avance III solids-300 MHz spectrometer operating at a frequency of 75 MHz for the ^{13}C nucleus. Approximately 80 mg of sample was placed into 4 mm zirconia rotors fitted with Kel-f® caps and spun in a double resonance H-X probehead at 8 kHz MAS (magic angle spinning). The ^{13}C and ^{1}H 90° radio frequency pulse lengths were optimized to 3.5 μs each. The ^{13}C spectra were acquired with 1 ms cross polarization contact time with a total suppression of spinning sidebands (TOSS) scheme, followed by ^{1}H decoupling at 75 kHz field strength using spinal-64 decoupling. The ^{13}C NQS (non-quaternary carbon suppression) spectra were recorded by turning off the ^{1}H decoupling for 40 μs during the TOSS period. For sufficient signal to noise, *ca.* 10 k transient were acquired for each sample with recycle delays of 3.0 s in between to ensure sufficient relaxation of the ^{1}H nuclei. The spectra were obtained at room temperature. The ^{13}C chemical shifts were referenced to the glycine CO peak at 176 ppm.

Magnetic measurements. Magnetic susceptibility data were collected on a Quantum Design Physical Property Measurement System (PPMS) with a Vibrating Sample Magnetometer (VSM) attachment. Measurements were taken at static and temperature-equilibrated 10 K intervals over the range 50-300 K, and at 0.25 K intervals over the range 2-50 K, under an applied field of 1 kOe. Kapton tape was used to seal the sample holder, which was cooled under vacuum. For reduced **1** and **2** (which are air sensitive), the sample was assembled in an Ar glove box and sealed under Ar for transport to the instrument. Diamagnetic corrections were calculated by measurement of the corresponding neutral polymers.

Fluorescence spectroscopy. Fluorescence data were collected on a Cary Varian Eclipse Fluorescence Spectrophotometer. Spectra were collected in the solid state by creating a flux of **2** in MeCN. Excitation wavelengths were determined by UV-vis spectra, and maximum excitations deduced from emission-excitation spectra. Confocal fluorescence microscopy was performed on an Olympus

FluoView FV1000 Confocal Microscope equipped with an Olympus LUCPLFL 40x/NA:0.6 air-immersion lens. Samples were excited using a 405 nm diode laser and emission spectra were collected in the range 420-600 nm.

DFT calculations. Standard DFT calculations were carried out with Gaussian 09.[30] Geometries were optimized at the B3-LYP/6-31G(d) level. Following each unconstrained geometry optimization, harmonic frequency analysis was carried out to confirm the nature of each stationary point as an equilibrium structure. For the structures **1mR** and **2mR**, the two triarylamine moieties were constrained to be perpendicular to the TzTz-type-core (TzTz for **1mR** and $C_2C_6H_4TzTzC_6H_4C_2$ for **2mR**), while all other coordinates were fully optimized. Improved single-point energies were evaluated using the M06-2X procedure[31] in conjunction with the 6-311+G(3df,2p) basis set. Electron affinities correspond to vertical values. In accordance with our previous studies,[32,33] the TD-BMK/6-31G(d) procedure[34] was employed to compute the UV-vis spectra of the model systems.

Acknowledgements

We gratefully acknowledge the support of the Australian Research Council.

Notes and references

[a]School of Chemistry, The University of Sydney, NSW 2006 (Australia). Tel: +61 (2) 9351 3777. E-mail: deanna.dalessandro@sydney.edu.au.
[b]NMR Facility, Mark Wainwright Analytical Centre, The University of New South Wales, 2052 (Australia).

1. G. Inzelt, M. Pineri, J. W. Schultze and M. A. Vorotyntsev, *Electrochim. Acta*, 2000, **45**, 2403.
2. D. Kumar and R. C. Sharma, *Eur. Polym. J.*, 1998, **34**, 1053.
3. I. H. Jung, J. Yu, E. Jeong, J. Kim, S. Kwon, H. Kong, K. Lee, H. Y. Woo and H. K. Shim, *Chem. Eur. J.*, 2010, **16**, 3743.
4. I. Osaka, R. Zhang, J. Liu, D.-M. Smilgies, T. Kowalewski and R. D. McCullough, *Chem. Mater.*, 2010, **22**, 4191.
5. T. W. Lee, N. S. Kang, J. W. Yu, M. H. Hoang, K. H. Kim, J. I. Jin and D. H. Choi, *J. Polym. Sci., Part A: Polym. Chem.*, 2010, **48**, 5921.
6. I. Osaka, M. Saito, T. Koganezawa and K. Takimiya, *Adv. Mater.*, 2013, **26**, 331.
7. I. Osaka, G. Sauve, R. Zhang, T. Kowalewski and R. D. McCullough, *Adv. Mater.*, 2007, **19**, 4160.
8. S. Van Mierloo, A. Hadipour, M. J. Spijkman, N. Van den Brande, B. Ruttens, J. Kesters, J. D'Haen, G. Van Assche, D. M. de Leeuw, T. Aernouts, J. Manca, L. Lutsen, D. J. Vanderzande and W. Maes, *Chem. Mater.*, 2012, **24**, 587.
9. A. J. Kronemeijer, E. Gili, M. Shahid, J. Rivnay, A. Salleo, M. Heeney and H. Sirringhaus, *Adv. Mater.*, 2012, **24**, 1558.
10. J. Weber, M. Antonietti and A. Thomas, *Macromolecules*, 2008, **41**, 2880.
11. O. K. Farha, A. M. Spokoyny, B. G. Hauser, Y.-S. Bae, S. E. Brown, R. Q. Snurr, C. A. Mirkin and J. T. Hupp, *Chem. Mater.*, 2009, **21**, 3033.
12. C. Hua, A. Rawal, T. B. Faust, P. D. Southon, R. Babarao, J. M. Hook and D. M. D'Alessandro, *J. Mater. Chem. A*, 2014, **2**, 12466.
13. Z. Xiang and D. Cao, *J. Mater. Chem. A*, 2013, **1**, 2691.
14. G. Distefano, H. Suzuki, M. Tsujimoto, S. Isoda, S. Bracco, A. Comotti, P. Sozzani, T. Uemura and S. Kitagawa, *Nat. Chem.*, 2013, **5**, 335.
15. Z. Xiang, D. Cao, W. Wang, W. Yang, B. Han and J. Lu, *J. Phys. Chem. C*, 2012, **116**, 5974.
16. A. Rajca, J. Wongsriratanakul, S. Rajca and R. Cerny, *Angew. Chem., Int. Ed.*, 1998, **37**, 1229.
17. H. Murata, D. Miyajima and H. Nishide, *Macromolecules*, 2006, **39**, 6331.
18. B. Z. Tang, Y. Geng, J. W. Y. Lam, B. Li, X. Jing, X. Wang, F. Wang, A. B. Pakhomov and X. X. Zhang, *Chem. Mat.*, 1999, **11**, 1581.
19. J. W. Colson and W. R. Dichtel, *Nat. Chem.*, 2013, **5**, 453.
20. H. Z. Akpinar, Y. A. Udum and L. Toppare, *J. Polym. Sci., Part A: Polym. Chem.*, 2013, **51**, 3901.
21. A. M. Bond, S. Fletcher, F. Marken, S. J. Shaw and P. G. Symons, *J. Chem. Soc., Faraday T.*, 1996, **92**, 3925.
22. J. L. Bredas, R. Silbey, D. S. Boudreaux and R. R. Chance, *J. Am. Chem. Soc.*, 1983, **105**, 6555.
23. Y. Li, Y. Cao, J. Gao, D. Wang, G. Yu and A. J. Heeger, *Synthetic Met.*, 1999, **99**, 243.
24. P. M. Usov, C. Fabian and D. M. D'Alessandro, *Chem. Commun.*, 2012, **48**, 3945.
25. N. G. Connelly and W. E. Geiger, *Chem. Rev.*, 1996, **96**, 877.
26. N. Niamnont, N. Kimpitak, K. Wongravee, P. Rashatasakhon, K. K. Baldridge, J. S. Siegel and M. Sukwattanasinitt, *Chem. Commun.*, 2013, **49**, 780.
27. D. R. Coulson, L. C. Satek and S. O. Grim, in *Inorg. Synth.*, John Wiley & Sons, Inc., 2007, pp. 121-124.
28. Y. Nakano, T. Yagyu, T. Hirayama, A. Ito and K. Tanaka, *Polyhedron*, 2005, **24**, 2141.
29. F. J. Rizzuto, T. B. Faust, B. Chan, C. Hua, D. M. D'Alessandro and C. J. Kepert, *Chem.-Eur. J.*, 2014, **20**, 17597.
30. M. J. Frisch, *et al.*, *Gaussian 09, Revision C.01*, Gaussian, Inc., Wallingford CT, 2009.
31. Y. Zhao and D. Truhlar, *Theor. Chem. Acc.*, 2008, **120**, 215.
32. C. F. Leong, B. Chan, T. B. Faust, P. Turner and D. M. D'Alessandro, *Inorg. Chem.*, 2013, **52**, 14246.
33. C. F. Leong, B. Chan, T. B. Faust and D. M. D'Alessandro, *Chem. Sci.*, 2014, **5**, 4724.
34. D. Boese and J. M. L. Martin, *J. Chem. Phys.*, 2004, **121**, 3405.

